下田健吾，木村真人，大久保善朗	拡散テンソルMRIを用いた認知障害を伴う老年期うつ病の検討	老年精神医学雑誌	19(増刊II)	199	2008
河嶌譲，齊藤卓弥，舘野周，成重竜一郎，御供正明，佐藤忠宏，大久保善朗	児童精神科医の不足と遠隔診療の可能性	精神神経学雑誌	S-183		2008
舘野周，大久保善朗	【アリピプラゾールの臨床】アリピプラゾールの薬理 Abi-Dargham のPET研究から	精神科	13(5)	401-405	2008
舘野周，大久保善朗	【痛みの精神医学】口腔内の痛み	臨床精神医学	37(1)	33-39	2008
原広一郎，大久保善朗	よく使う日常治療薬の正しい使い方　抗てんかん薬の使い方	レジデントノート	9(12)	1789-1793	2008
荒川亮介，奥村正紀，伊藤浩，高橋英彦，高野晴成，関千江，大久保善朗，須原哲也	(S,S)-[18F]FMeNER-D2による脳内ノルエピネフリントランスポーターの定量	核医学	45(3)	S227	2008
上田諭，河嶌譲，齊藤卓弥，野上毅，花尻美和，下田健吾，大久保善朗	重度の制止に対しECTのみで効果がみられずベンゾジアゼピン併用後に劇的に改善したうつ病の一例	精神科治療学	23(7)	885-890	2008
上田諭，児玉由希絵，大久保善朗，伊藤敬雄	眼球彷徨roving eye movementが観察されほどなく死に至った2症例　せん妄増悪時の特徴的眼球運動	精神医学	50(11)	1103-1106	2008
上田諭，西川律子，伊藤敬雄，大久保善朗，岩井美幸，岡崎怜子	私のカルテから 術後抑うつに対するsulpiride100mg/日投与で顕著な筋固縮を生じADL回復が遅れた高齢者症例　リエゾン活動での経験	精神医学	50(10)	1021-1024	2008
上田諭，大久保善朗	長年のセネストパチーが躁状態ないし混合状態への治療で改善した2症例	老年精神医学雑誌	19(増刊II)	160	2008
川島義高，伊藤敬雄，舘野周，下田健吾，鈴木博子，山本正浩，池森紀夫，大久保善朗	解離症状下での自殺企図及び自傷行為　救命救急センターに搬送された9症例	日本社会精神医学会雑誌	17(1)	134	2008

川島義高，光井和馬，伊藤敬雄，大久保善朗，増野智彦，近藤久禎，久志本成樹，川井真，横田裕行，山本保博	自殺企図および自傷行為にて高度救命救急センターに搬送された症例の実態報告　在院期間と精神科介入期間	日本臨床救急医学会雑誌	11(2)	252	2008
大久保善朗	精神医学の卒前教育を考える医学教育モデル・コア・カリキュラムについて	精神神経学雑誌	S-265		2008
八幡憲明，高橋英彦，鈴木秀典，大久保善朗	ヒト注意機構に対して選択的セロトニン再取り込み阻害薬が及ぼす効果に関する薬理学的 fMRI 研究	日本薬理学雑誌	131(1)	15	2008
鈴木雅之，一宮哲哉，新貝慈利，児玉由希絵，上田論，下田健吾，大久保善朗	片側性 ECT が奏効した高齢者うつ病の 2 症例	精神神経学雑誌	110(4)	342	2008
原広一郎，足立直人，松浦雅人，原常勝，小穴康功，大久保善朗，村松玲美，加藤昌明，大沼悌一	精神病を伴うてんかん症例における利き手	てんかん研究	26(3)	403-410	2009
森山泰、村松太郎、加藤元一郎、秋山知子、仲地良子、三村將、鹿島晴雄	アルツハイマー型認知症における表情認知と精神症状・行動障害との関連について	臨床精神医学	37	315-320	2008
船山道隆、加藤元一郎、三村　將	地理的定位錯誤から重複記憶錯誤に発展した右前頭葉出血の１例　～重複記憶錯誤の成立過程について～	高次脳機能研究	28 (4)	383-391	2008
斎藤文恵、加藤元一郎、村松太郎、藤永直美、吉野真理子、鹿島晴雄	アルツハイマー病に出現した漢字の選択的失書について	高次脳機能研究	28(4)	392-403	2008
船山道隆、前田貴記、三村　將、加藤元一郎	両側前頭葉損傷に出現した forced gazing（強制凝視）について	高次脳機能研究	29 (1)	40-48	2009
加藤元一郎	アルツハイマー病の診断―神経心理学的検査	日本臨床	６６号増刊号	264-269	2008
加藤元一郎	アルツハイマー病の治療・管理―現実見当識訓練	日本臨床	６６号増刊号	383-386	2008

加藤元一郎、林海香、野崎昭子	アスペルガー症候群と統合失調症辺縁群における神経心理学的問題と脳画像所見	精神科治療学	23	173-181	2008
加藤元一郎	記憶錯誤	こころの科学	(March 3) 138	78-84	2008
加藤元一郎、秋山」知子	顔、表情、視線の認知と扁桃体	Clinical Neuroscience	26	413-415	2008
船山道隆、加藤元一郎	前頭葉と自律性の障害－特に強制行動と病的収集活動について	分子精神医学	8 (2)	125-131	2008
大川原浩、吉野文浩、加藤元一郎	変性性認知症—アルツハイマー病について	Monthly Book Medical Rehabilitation	91	34-40	2008
林　海香、五十嵐一枝、加藤元一郎	神経心理学的観点から見た広汎性発達障害と統合失調症の差異—特にアスペルガー症候群における優れた推論能力について	最新精神医学	13(3)	249-255	2008
加藤元一郎	遂行機能障害とその検査	神経内科	68 (Suppl 5)	523-531	2008
加藤元一郎	前頭葉機能障害の診かた	神経心理学	24	96-108	2008
加藤元一郎	記憶とその病態	高次脳機能研究	28	206-213	2008
高畑圭輔、加藤元一郎	自閉性サバァンと獲得性サバァンの神経基盤	BARIN and NERVE	60	861-869	2008
加藤元一郎	アルコール依存症の診断基準とは？	肥満と糖尿病	7	563-565	2008

渡邊 衡一郎, 田 亮介, 加藤 元一郎	うつ病の回復過程におけるドパミンの役割	臨床薬理の進歩	29	226-231	2008
渡邊 衡一郎, 田 亮介、加藤 元一郎	諸外国のうつ病治療ガイドライン・アルゴリズムにおける新規抗うつ薬の位置づけ－諸外国でもSSRI, SNRIは第一選択薬なのか	臨床精神薬理	11(10)	1849-1859	2008
加藤元一郎、田渕肇	成人トゥレット症候群における認知障害、脳機能画像、強迫症状に関する研究	トゥレット研究会会誌第１４回研究会報告号	3月10日		2008
加藤元一郎	アスペルガー症候群の認知障害、脳画像所見、及び臨床症状の特徴について	臨床精神病理	29	287-296	2008
加藤元一郎	脳損傷と認知リハビリテーション	Jpn J Neurosurg (Tokyo)(脳神経外科ジャーナル)	18	277-285	2009

Ⅳ. 研究成果の刊行物・別刷

Quantitative Analysis of Norepinephrine Transporter in the Human Brain Using PET with (S,S)-^{18}F-FMeNER-D_2

Ryosuke Arakawa[1,2], Masaki Okumura[1,2], Hiroshi Ito[1], Chie Seki[1], Hidehiko Takahashi[1], Harumasa Takano[1], Ryuji Nakao[3], Kazutoshi Suzuki[3], Yoshiro Okubo[2], Christer Halldin[4], and Tetsuya Suhara[1]

[1]Molecular Neuroimaging Group, Molecular Imaging Center, National Institute of Radiological Sciences, Chiba, Japan; [2]Department of Neuropsychiatry, Nippon Medical School, Tokyo, Japan; [3]Molecular Probe Group, Molecular Imaging Center, National Institute of Radiological Sciences, Chiba, Japan; and [4]Psychiatry Section, Department of Clinical Neuroscience, Karolinska Institutet, Karolinska Hospital, Stockholm, Sweden

(S,S)-^{18}F-FMeNER-D_2 was recently developed as a radioligand for the measurement of norepinephrine transporter imaging with PET. In this study, a norepinephrine transporter was visualized in the human brain using this radioligand with PET and quantified by several methods. **Methods:** PET scans were performed on 10 healthy men after intravenous injection of (S,S)-^{18}F-FMeNER-D_2. Binding potential relative to nondisplaceable binding (BP_{ND}) was quantified by the indirect kinetic, simplified reference-tissue model (SRTM), multilinear reference-tissue model (MRTM), and ratio methods. The indirect kinetic method was used as the gold standard and was compared with the SRTM method with scan times of 240 and 180 min, the MRTM method with a scan time of 240 min, and the ratio method with a time integration interval of 120–180 min. The caudate was used as reference brain region. **Results:** Regional radioactivity was highest in the thalamus and lowest in the caudate during PET scanning. BP_{ND} values by the indirect kinetic method were 0.54 ± 0.19 and 0.35 ± 0.25 in the thalamus and locus coeruleus, respectively. BP_{ND} values found by the SRTM, MRTM, and ratio methods agreed with the values demonstrated by the indirect kinetic method (r = 0.81–0.92). **Conclusion:** The regional distribution of (S,S)-^{18}F-FMeNER-D_2 in our study agreed with that demonstrated by previous PET and postmortem studies of norepinephrine transporter in the human brain. The ratio method with a time integration interval of 120–180 min will be useful for clinical research of psychiatric disorders for estimation of norepinephrine transporter occupancy by antidepressants without requiring arterial blood sampling and dynamic PET.

Key Words: norepinephrine transporter; (S,S)-^{18}F-FMeNER-D_2; positron emission tomography; human brain; thalamus

J Nucl Med 2008; 49:1270–1276
DOI: 10.2967/jnumed.108.051292

Received Jan. 30, 2008; revision accepted May 2, 2008.
For correspondence or reprints contact: Hiroshi Ito, Molecular Neuroimaging Group, Molecular Imaging Center, National Institute of Radiological Sciences, 4-9-1, Anagawa, Inage-ku, Chiba, 263-8555, Japan.
E-mail: hito@nirs.go.jp

Norepinephrine, one of the monoamine neurotransmitters in the central nervous system, has been reported to be related to several functions such as memory, cognition, consciousness, and emotion and to play important roles in psychiatric disorders (*1–4*). Norepinephrine transporter is responsible for the reuptake of norepinephrine into presynaptic nerves. Norepinephrine reuptake inhibitors are used for the treatment of depression and attention deficit hyperactivity disorder (ADHD) (*4–7*). Thus, changes in norepinephrine transporter functions in several psychiatric disorders can be expected, but in vivo estimation has not been performed because of a lack of suitable radioligands for norepinephrine transporters.

(S,S)-^{18}F-FMeNER-D_2 has recently been developed as a radioligand for the measurement of norepinephrine transporter for PET (*8*). (S,S)-^{18}F-FMeNER-D_2 is a reboxetine analog and has high affinity for norepinephrine transporter and high selectivity from other monoamine transporters. Tracer distribution and dosimetry of (S,S)-^{18}F-FMeNER-D_2 were reported in monkey (*8,9*) and human studies (*10,11*). Another monkey study showed that (S,S)-^{18}F-FMeNER-D_2 binding decreased by the administration of atomoxetine, a selective norepinephrine reuptake inhibitor (*12*). However, quantitative analyses of (S,S)-^{18}F-FMeNER-D_2 bindings using an arterial input function have not yet, to our knowledge, been performed.

In this study, we aimed to quantify the norepinephrine transporter bindings in the human brain using (S,S)-^{18}F-FMeNER-D_2 with arterial blood sampling and also to validate noninvasive methods for quantification without arterial blood sampling.

MATERIALS AND METHODS

Subjects

Ten healthy men (age range, 21–26 y; mean ± SD, 22.7 ± 1.6 y) participated in this study. All subjects were free of any somatic, neurologic, or psychiatric disorders, and they had no

history of current or previous drug abuse. Written informed consent was obtained from all subjects following a complete description of this study. The study was approved by the Ethics and Radiation Safety Committee of the National Institute of Radiologic Sciences, Chiba, Japan.

PET Procedure

(S,S)-^{18}F-FMeNER-D_2 was synthesized by fluoromethylation of nor-ethyl-reboxetine with ^{18}F-bromofluoromethane-d_2 as previously described (*8*). A PET scanner system (ECAT EXACT HR+; CTI-Siemens) was used for all subjects, with a head holder used to minimize head movement. A transmission scan for attenuation correction was performed using a ^{68}Ge–^{68}Ga source. Dynamic PET scans were performed after a 1-min intravenous slow bolus injection of 353.4–382.7 MBq (mean ± SD, 368.1 ± 9.1 MBq) of (S,S)-^{18}F-FMeNER-D_2. The specific radioactivity of (S,S)-^{18}F-FMeNER-D_2 was 144.8–390.2 GBq/μmol (312.8 ± 76.2 GBq/μmol). Brain radioactivities were measured from 0 to 90 min (1 min × 10, 2 min × 15, and 5 min × 10), from 120 to 180 min (10 min × 6), and from 210 to 240 min (10 min × 3). MR images of the brain were acquired with a 1.5-T MRI scanner (Gyroscan NT; Philips). T1-weighted images were obtained at 1-mm slices.

Arterial Blood Sampling and Metabolite Analysis

To obtain the arterial input function, arterial blood samples were taken manually 42 times during the PET scan. Each blood sample was centrifuged to obtain plasma and blood cell fractions, and the concentrations of radioactivity in whole blood and in plasma were measured.

The percentage of unchanged (S,S)-^{18}F-FMeNER-D_2 in plasma was determined by high-performance liquid chromatography in 22 of the blood samples. Acetonitrile was added to each plasma sample, and samples were centrifuged. The supernatant was subjected to high-performance liquid chromatography radiodetection analysis (column: XBridge Prep C18, mobile phase, 90% acetonitrile/50 mM ammonium acetate = 48/52; Waters). Plasma input function was defined as radioactivity of plasma multiplied by the percentage of unchanged radioligand.

Regions of Interest

All MR images were coregistered to the PET images using a statistical parametric mapping system (SPM2; The Wellcome Trust Centre for Neuroimaging, University College London). Regions of interest were drawn manually on summed PET images, with reference to coregistered MR images, and were defined for the thalamus, locus coeruleus, hippocampus, anterior cingulate gyrus, and caudate head. Regional radioactivity was calculated for each frame, corrected for decay, and plotted versus time.

Kinetic Model of ^{18}F-FMeNER-D_2

To describe the kinetics of (S,S)-^{18}F-FMeNER-D_2 in the brain, the 3-compartment model with 4 first-order rate constants was used. The 3 compartments were defined as follows: C_P was the radioactivity concentration of unchanged radioligand in plasma (arterial input function), C_{ND} was the radioactivity concentration of nondisplaceable radioligand in the brain, including nonspecifically bound and free radioligand, and C_S was the radioactivity concentration of radioligand specifically bound to transporters. The rate constants K_1 and k_2 represent the influx and efflux rates, respectively, for radioligand diffusion through the blood–brain barrier, and the rate constants k_3 and k_4 are the radioligand transfers between the compartments for nondisplaceable and specifically bound radioligand, respectively. This model can be described by the following equations:

$$\frac{dC_{ND}(t)}{dt} = K_1C_P(t) - (k_2+k_3)C_{ND}(t) + k_4C_S(t),$$

$$\frac{dC_S(t)}{dt} = k_3C_{ND}(t) - k_4C_S(t), \text{ and}$$

$$C_T(t) = C_{ND}(t)+C_S(t).$$

$C_T(t)$ is the total radioactivity concentration in any brain region measured by PET.

Calculation of (S,S)-^{18}F-FMeNER-D_2 Binding Potential

(S,S)-^{18}F-FMeNER-D_2 binding was quantified by the indirect kinetic, simplified reference-tissue model (SRTM), multilinear reference-tissue model (MRTM), and ratio methods. In these methods, (S,S)-^{18}F-FMeNER-D_2 bindings were expressed as binding potentials relative to nondisplaceable binding (BP_{ND}) (*13*). We used the caudate as the reference brain region because of its

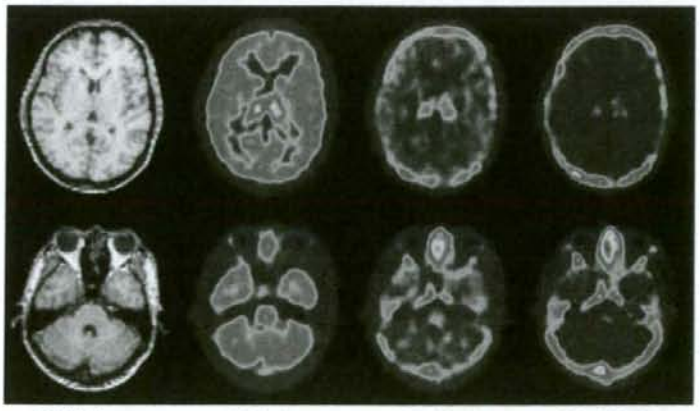

FIGURE 1. Typical summed PET images of (S,S)-^{18}F-FMeNER-D_2 and T1-weighted MR images. Upper panel shows slice of caudate and thalamus, and lower panel shows slice of locus coeruleus.

negligible norepinephrine transporter density (*14–16*). Software (PMOD; PMOD Technologies) was used for these analyses.

Indirect Kinetic Method

With the caudate as reference region, BP_{ND} can be expressed as:

$$BP_{ND} = \frac{V_{T(regions)}}{V_{T(caudate)}} - 1,$$

where $V_{T(regions)}$ is the total distribution volume (= $[K_1/k_2][k_3/k_4 + 1]$) of target regions and $V_{T(caudate)}$ is the total distribution volume of the caudate. The K_1, k_2, k_3, and k_4 values were determined by nonlinear least-squares curve fitting to the regional time–activity curves. In this analysis, blood volume (V_b), which depends on the first-pass extraction fraction of the tracer, was also estimated using the radioactivity of whole blood to diminish the influence of the tracer remaining in the blood. In this study, the indirect kinetic method was used as the standard method (*17*).

SRTM Method

Assuming that both target and reference regions have the same level of nondisplaceable binding, the SRTM method can be used to describe time–activity data in the target region as follows (*18*):

$$C_T(t) = R_1 C_R(t) + \left(k_2 - R_1 \frac{k_2}{1+BP_{ND}}\right) C_R(t) \otimes \exp\left(\frac{-k_2}{1+BP_{ND}} t\right),$$

where R_1 is the ratio of K_1/K_1' (K_1, influx rate constant for the brain region; K_1', influx rate constant for the reference region), $C_R(t)$ is the radioactivity concentration in the reference region (caudate), and $\otimes$ denotes the convolution integral. Using this model, 3 parameters (R_1, k_2, and BP_{ND}) were estimated by a nonlinear curve-fitting procedure. Scan data up to 180 or 240 min were used.

MRTM Method

The MRTM method is one of the variations of the graphical approaches (*19*). After a certain equilibrium time (t*), the following multilinear regression is obtained:

$$C_T(T) = -\frac{V_{T(regions)}}{V_{T(caudate)}} \int_0^T C_R(t)dt + \frac{1}{b} \int_0^T C_T(t)dt - \frac{V_{T(regions)}}{V_{T(caudate)} k_2' b} C_R(T),$$

where k_2' is the efflux rate constant for the reference region. In this analysis, t* was determined so that the maximum error from the regression within the linear segment would be 10% for each time–activity curve. BP_{ND} for the MRTM method was calculated using the same equation as described previously for the indirect kinetic method (= $V_{T(regions)}/V_{T(caudate)} - 1$). Scan data up to 240 min were used.

Ratio Method

In the ratio method, BP_{ND} can be expressed as:

$$BP_{ND} = \frac{AUC_{(regions)}}{AUC_{(caudate)}} - 1,$$

where $AUC_{(regions)}$ is the area under the time–activity curve of the target regions and $AUC_{(caudate)}$ is the area under the time–activity curve of the caudate. The integration interval of 120–180 min was used in this method.

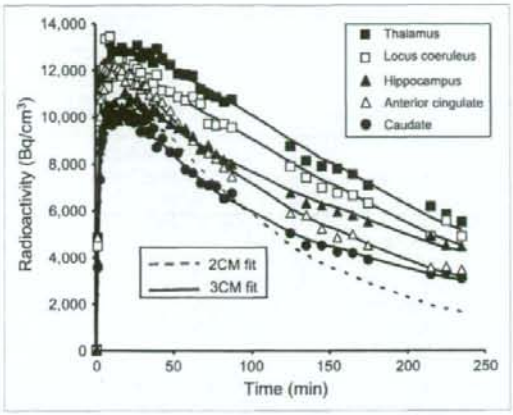

FIGURE 2. Typical time–activity curves of (S,S)-^{18}F-FMeNER-D_2 in brain. Time–activity curves of all regions could be described by 3-compartment model (3CM). Time–activity curve of caudate could also be described by 2-compartment model (2CM).

Simulation Study

A simulation study was performed to estimate errors in BP_{ND} calculated by the SRTM and ratio methods. Tissue time–activity curves for the thalamus were generated using the 3-compartment model. The rate constant values K_1, k_2, and k_4 of the thalamus were assumed to be 0.157, 0.037, and 0.016, respectively. The value of k_3 ranged from 0.019 to 0.039 in 6 steps. Tissue time–activity curves for the caudate were also generated using the 3-compartment model, assuming that the rate constant values K_1, k_2, k_3, and k_4 were 0.124, 0.032, 0.010, and 0.010, respectively. These assumed values were taken from the results obtained by the kinetic approach. The average of arterial input function for all

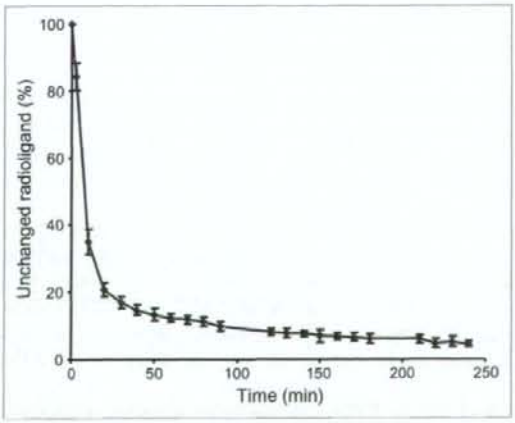

FIGURE 3. Average percentage of unchanged (S,S)-^{18}F-FMeNER-D_2 in plasma. Bars indicate 1 SD.

TABLE 1
Data for Each Brain Region Determined by Kinetic Approach Using 3-Compartment Model with Arterial Input Function

Region	V_b	Rate constant				V_{ND}	V_T
		K_1 (mL/mL/min)	k_2 (min^{-1})	k_3 (min^{-1})	k_4 (min^{-1})		
Thalamus	0.045 ± 0.016	0.157 ± 0.025	0.037 ± 0.005	0.027 ± 0.007	0.016 ± 0.002	4.36 ± 0.90	11.45 ± 2.29
Locus coeruleus	0.032 ± 0.008	0.154 ± 0.026	0.040 ± 0.009	0.020 ± 0.008	0.013 ± 0.004	4.06 ± 1.01	9.89 ± 1.78
Hippocampus	0.038 ± 0.010	0.119 ± 0.013	0.035 ± 0.011	0.022 ± 0.016	0.015 ± 0.005	3.73 ± 0.83	8.48 ± 1.14
Anterior cingulate	0.053 ± 0.011	0.144 ± 0.019	0.032 ± 0.005	0.010 ± 0.005	0.012 ± 0.004	4.61 ± 1.04	8.33 ± 1.70
Caudate (3-compartment model)	0.031 ± 0.008	0.124 ± 0.018	0.032 ± 0.005	0.010 ± 0.005	0.010 ± 0.004	3.92 ± 0.80	7.51 ± 1.51
Caudate (2-compartment model)	0.045 ± 0.010	0.109 ± 0.017	0.019 ± 0.001			5.77 ± 0.98	

Values are mean ± SD. V_{ND} is defined as K_1/k_2 and V_T as $(K_1/k_2)(k_3/k_4 + 1)$.

subjects was used to generate the time–activity curves. With these generated time–activity curves, BP_{ND} values were calculated by the SRTM (scan time of 240 min), MRTM, and ratio methods. The calculated BP_{ND} values for the simulation study were compared with those calculated by the indirect kinetic method.

RESULTS

Typical summed PET images of 3 time periods and T1-weighted MR images are shown in Figure 1. Typical time–activity curves in the brain showed that regional radioactivity was highest in the thalamus and lowest in the caudate (Fig. 2). Time–activity curves for all regions could be described by the 3-compartment model. The time–activity curve for the caudate could also be described by the 2-compartment model. The average percentage of unchanged (S,S)-^{18}F-FMeNER-D_2 in plasma was 84.4% ± 3.9% at 3 min, 35.1% ± 3.7% at 10 min, 10.0% ± 1.4% at 90 min, 6.1% ± 1.3% at 180 min, and 4.5% ± 0.9% at 240 min (Fig. 3).

The blood volume, rate constants, nondisplaceable distribution volume (V_{ND}), and total distribution volume (V_T) for each brain region determined by the kinetic approach using the 3-compartment model with arterial input function are shown in Table 1. For the caudate, the 2-compartment model without a specific binding compartment was also applied. Akaike information criteria of the 3-compartment model were lower than those of the 2-compartment model (143 ± 16 vs. 227 ± 6, $P < 0.0001$; paired t statistics).

The BP_{ND} values of the thalamus calculated by all methods are shown in Table 2. BP_{ND} values in the thalamus by the MRTM method showed the best correlation with those by the indirect kinetic method ($r = 0.92$) (Fig. 4C). The SRTM method with scan times of 180 and 240 min and the ratio method also agreed with the BP_{ND} values by the indirect kinetic method ($r = 0.81$–0.91) (Figs. 4A, 4B, and 4D). However, BP_{ND} values in brain regions other than the thalamus could not be estimated by the SRTM and MRTM methods because of failed curve fitting, showing no convergence. The BP_{ND} values of each brain region by the indirect kinetic and ratio methods are shown in Table 3. The correlation of BP_{ND} values in all target regions between the indirect kinetic and the ratio methods is shown in Figure 5A. The Bland–Altman plot of BP_{ND} values by these 2 methods is shown in Figure 5B.

In the simulation study, estimated BP_{ND} values, compared with assumed BP_{ND} values, by the SRTM (scan time of 240 min), MRTM, and ratio methods were slightly overestimated (Fig. 6).

DISCUSSION

After intravenous injection of (S,S)-^{18}F-FMeNER-D_2, radioactivity was highest in the thalamus and lowest in the caudate. BP_{ND} in the thalamus using the ratio method was 0.67 ± 0.15, almost the same value as found in a previous human PET study (*10*). The locus coeruleus showed relatively high uptake, and the hippocampus and anterior cingulate cortex showed relatively low uptake. This result was in agreement with previous reports that the thalamus and locus coeruleus showed high densities of norepinephrine transporters (*14–16,20*). Previous autoradiographic studies with human postmortem brains reported that norepinephrine transporter density in the locus coeruleus was higher by about 10 times than that in the thalamus (*14,15*). However,

TABLE 2
BP_{ND} Values in Thalamus by All Methods

Method	BP_{ND}
Indirect kinetic	0.54 ± 0.19
SRTM (240 min)	0.61 ± 0.14
SRTM (180 min)	0.64 ± 0.14
MRTM	0.61 ± 0.14
Ratio	0.67 ± 0.15

Values are mean ± SD.

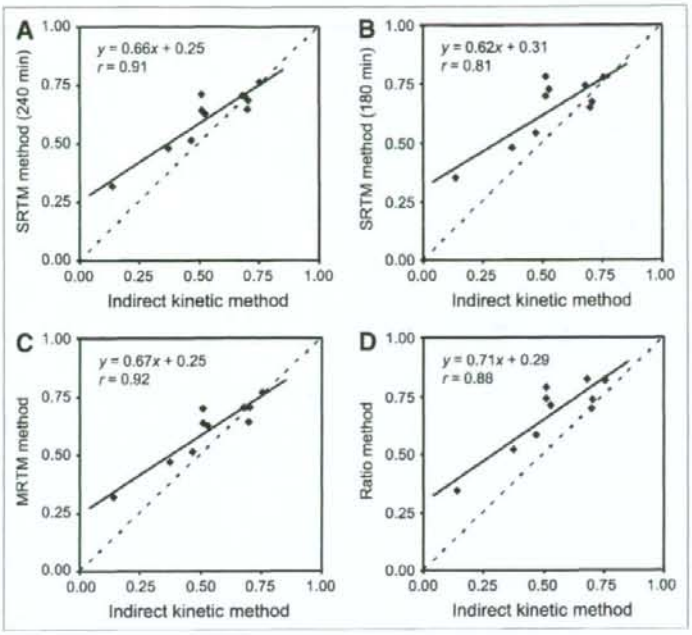

FIGURE 4. Correlation between BP_{ND} values in thalamus estimated by indirect kinetic method and SRTM method with scan time of 240 min (A) or 180 min (B), MRTM method (C), or ratio method (D).

previous and present PET studies reported almost the same values between the locus coeruleus and thalamus (*10,16*). One possible reason for the discrepancy was the partial-volume effect due to the limited spatial resolution of the PET scanner, the locus coeruleus being a very small structure.

In the current study, the indirect kinetic method with arterial blood sampling was used as the standard method (*17*). The BP_{ND} values in the thalamus by the other 3 methods—the SRTM with scan times of 240 and 180 min, MRTM, and ratio methods—were in agreement with those found by the indirect kinetic method. Although the indirect kinetic method was considered the standard method, it required a long PET time as well as arterial blood sampling, an invasive procedure particularly unsuitable for patients with psychiatric disorders. Because the ratio method does not require long PET and arterial blood sampling, this method would be preferable for clinical investigation. The SRTM and MRTM methods can estimate only the thalamus, as curve fitting failed in other brain regions. The MRTM2 method (*19*) may be able to estimate BP_{ND} in regions other than thalamus; however, weighted k_2' value among brain regions could not be calculated in this tracer. The possible reasons of failed curve fitting might be the small differences of time–activity curves between target and reference regions and the noise in time–activity curves. The ratio method could reveal BP_{ND} values in brain regions other than the thalamus. The BP_{ND} values by the ratio method were in agreement with those by the indirect kinetic method for all brain regions (Fig. 5A). Although bias was observed by the ratio method, this bias did not change according to the BP_{ND} values (Fig. 5B). The ratio method could estimate norepinephrine transporter binding in the thalamus and also other brain regions.

The time–activity curves in the caudate were better described by the 3-compartment model than the 2-compartment model. Similar results were reported for several PET radioligands; the kinetics in the reference region were also evaluated using the 3-compartment model (*17,21,22*). The results could be explained if the caudate contained specific binding for norepinephrine transporters. However, previous autoradiographic studies showed that the density of norepinephrine transporters in the caudate was very low (*14–16*). Another possible explanation is that the compartments of free and nonspecific binding could be separated by the kinetic analysis. Moreover, spillover from

TABLE 3
BP_{ND} Values for Each Brain Region by Indirect Kinetic and Ratio Methods

Region	Indirect kinetic method	Ratio method
Thalamus	0.54 ± 0.19	0.67 ± 0.15
Locus coeruleus	0.35 ± 0.25	0.42 ± 0.13
Hippocampus	0.13 ± 0.14	0.23 ± 0.09
Anterior cingulate	0.13 ± 0.16	0.15 ± 0.09

Values are mean ± SD.

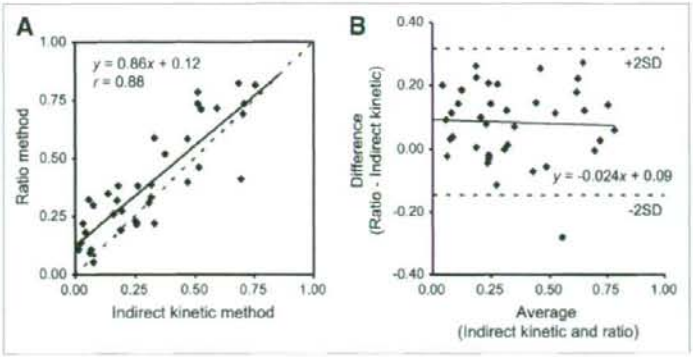

FIGURE 5. Correlation between BP_{ND} values in all target regions estimated by indirect kinetic method and ratio method (A) and Bland–Altman plot (B).

other brain regions to the caudate may affect the results because the caudate is a small structure and is surrounded by regions with specific binding.

In this study, we investigated norepinephrine transporter binding in only limited regions. Other brain regions such as the cerebral cortex and cerebellum are also considered to possess norepinephrine neurons and norepinephrine transporters (*14–16*). However, (S,S)-^{18}F-FMeNER-D_2 showed that defluorination and uptake of ^{18}F in the skull influenced cerebral radioactivity (*8*). Although (S,S)-^{18}F-FMeNER-D_2 had reduced defluorination by the dideuteration, compared with (S,S)-^{18}F-FMeNER, estimation in the cerebral cortex or cerebellum adjacent to the skull was considered difficult.

In this study, occupancy of norepinephrine transporter by antidepressants was not evaluated. Previous animal studies showed dose-dependent norepinephrine transporter occupancy by atomoxetine (*12*). However, a human study using [^{11}C](S,S)-MRB reported no differences in occupancy between different doses of atomoxetine (*16*). Further, occupancy studies in humans to estimate the clinical effects of antidepressants, similar to occupancy studies for dopamine D_2 receptor and serotonin transporters (*23,24*), will be needed.

In the simulation study, BP_{ND} values by the SRTM with a scan time of 240 min, MRTM, and the ratio methods were overestimated, compared with assumed BP_{ND} (Fig. 6). Such overestimation was also observed in measured PET data, especially in regions with low specific binding (Figs. 4A, 4C, and 4D). The degree of overestimation of BP_{ND} was larger in measured data than that in the simulation, especially in regions with low specific binding. Noise in measured data might cause such discrepancy, and therefore further studies using simulated data with added noise may be required. Although linear correlation was observed in BP_{ND} values between the ratio and indirect kinetic methods, this overestimation may cause errors in the calculation of occupancy by antidepressants. When baseline BP_{ND} is 0.6, estimated occupancy by the ratio method is 22%, 43%, and 65%, corresponding to the assumed occupancy of 25%, 50%, and 75%, respectively (Fig. 6). The SRTM and MRTM methods also showed the underestimation of occupancy, 21%, 43%, and 64% by the former and 21%, 42%, and 63% by the latter.

CONCLUSION

(S,S)-^{18}F-FMeNER-D_2 is a suitable radioligand for PET measurement of norepinephrine transporters in the human brain. The 3-compartment model could well describe the brain kinetics of (S,S)-^{18}F-FMeNER-D_2. Because the ratio method does not require long PET imaging times and arterial blood sampling, this method would be useful for clinical research of psychiatric disorders.

ACKNOWLEDGMENTS

We thank Dr. Fumitoshi Kodaka, Dr. Tatsui Otsuka, Katsuyuki Tanimoto, Takahiro Shiraishi, and Akira Ando

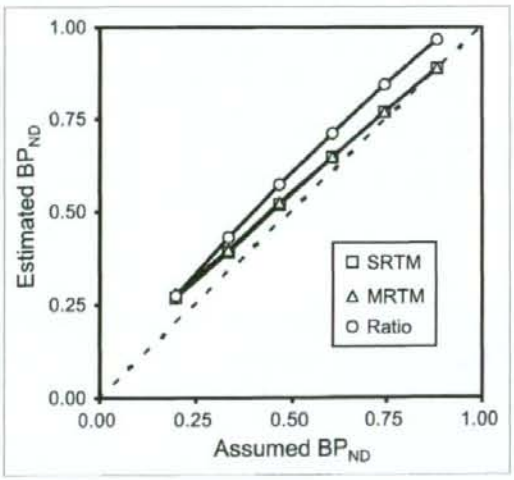

FIGURE 6. Correlations between assumed BP_{ND} values by indirect kinetic method and those by SRTM with scan time of 240 min, MRTM method, or ratio method in simulation studies.

for their assistance in performing the PET experiments at the National Institute of Radiological Sciences. We also thank Yoshiko Fukushima of the National Institute of Radiological Sciences for her help as clinical research coordinator. This study was supported by a consignment expense for the Molecular Imaging Program on Research Base for PET Diagnosis from the Ministry of Education, Culture, Sports, Science and Technology (MEXT), Japanese government, and by a Health and Labor Sciences Research Grant for Research on Psychiatric and Neurological Diseases and Mental Health from the Ministry of Health, Labor and Welfare, Japanese government.

REFERENCES

1. Harmer CJ, Shelley NC, Cowen PJ, Goodwin GM. Increased positive versus negative affective perception and memory in healthy volunteers following selective serotonin and norepinephrine reuptake inhibition. *Am J Psychiatry.* 2004;161:1256–1263.
2. Strange BA, Hurlemann R, Dolan RJ. An emotion-induced retrograde amnesia in humans is amygdala- and beta-adrenergic-dependent. *Proc Natl Acad Sci USA.* 2003;100:13626–13631.
3. Southwick SM, Davis M, Horner B, et al. Relationship of enhanced norepinephrine activity during memory consolidation to enhanced long-term memory in humans. *Am J Psychiatry.* 2002;159:1420–1422.
4. Nutt DJ. The role of dopamine and norepinephrine in depression and antidepressant treatment. *J Clin Psychiatry.* 2006;67(suppl 6):3–8.
5. Cheng JY, Chen RY, Ko JS, Ng EM. Efficacy and safety of atomoxetine for attention-deficit/hyperactivity disorder in children and adolescents: meta-analysis and meta-regression analysis. *Psychopharmacology (Berl).* 2007;194:197–209.
6. Chamberlain SR, Del Campo N, Dowson J, et al. Atomoxetine improved response inhibition in adults with attention deficit/hyperactivity disorder. *Biol Psychiatry.* 2007;62:977–984.
7. Shelton RC. The dual-action hypothesis: does pharmacology matter? *J Clin Psychiatry.* 2004;65(suppl 17):5–10.
8. Schou M, Halldin C, Sovago J, et al. PET evaluation of novel radiofluorinated reboxetine analogs as norepinephrine transporter probes in the monkey brain. *Synapse.* 2004;53:57–67.
9. Seneca N, Andree B, Sjoholm N, et al. Whole-body biodistribution, radiation dosimetry estimates for the PET norepinephrine transporter probe (*S,S*)-[^{18}F]FMeNER-D2 in non-human primates. *Nucl Med Commun.* 2005;26:695–700.
10. Takano A, Gulyas B, Varrone A, et al. Imaging the norepinephrine transporter with positron emission tomography: initial human studies with (*S,S*)-[^{18}F]FMeNER-D$_2$. *Eur J Nucl Med Mol Imaging.* 2008;35:153–157.
11. Takano A, Halldin C, Varrone A, et al. Biodistribution and radiation dosimetry of the norepinephrine transporter radioligand (*S,S*)-[^{18}F]FMeNER-D$_2$: a human whole-body PET study. *Eur J Nucl Med Mol Imaging.* 2008;35:630–636.
12. Seneca N, Gulyas B, Varrone A, et al. Atomoxetine occupies the norepinephrine transporter in a dose-dependent fashion: a PET study in nonhuman primate brain using (*S,S*)-[^{18}F]FMeNER-D2. *Psychopharmacology (Berl).* 2006;188:119–127.
13. Innis RB, Cunningham VJ, Delforge J, et al. Consensus nomenclature for in vivo imaging of reversibly binding radioligands. *J Cereb Blood Flow Metab.* 2007;27:1533–1539.
14. Schou M, Halldin C, Pike VW, et al. Post-mortem human brain autoradiography of the norepinephrine transporter using (*S,S*)-[^{18}F]FMeNER-D2. *Eur Neuropsychopharmacol.* 2005;15:517–520.
15. Donnan GA, Kaczmarczyk SJ, Paxinos G, et al. Distribution of catecholamine uptake sites in human brain as determined by quantitative [^{3}H] mazindol autoradiography. *J Comp Neurol.* 1991;304:419–434.
16. Logan J, Wang GJ, Telang F, et al. Imaging the norepinephrine transporter in humans with (*S,S*)-[^{11}C]O-methyl reboxetine and PET: problems and progress. *Nucl Med Biol.* 2007;34:667–679.
17. Ito H, Sudo Y, Suhara T, Okubo Y, Halldin C, Farde L. Error analysis for quantification of [^{11}C]FLB 457 binding to extrastriatal D_2 dopamine receptors in the human brain. *Neuroimage.* 2001;13:531–539.
18. Lammertsma AA, Hume SP. Simplified reference tissue model for PET receptor studies. *Neuroimage.* 1996;4:153–158.
19. Ichise M, Liow JS, Lu JQ, et al. Linearized reference tissue parametric imaging methods: application to [^{11}C]DASB positron emission tomography studies of the serotonin transporter in human brain. *J Cereb Blood Flow Metab.* 2003;23:1096–1112.
20. Ordway GA, Stockmeier CA, Cason GW, Klimek V. Pharmacology and distribution of norepinephrine transporters in the human locus coeruleus and raphe nuclei. *J Neurosci.* 1997;17:1710–1719.
21. Lundberg J, Odano I, Olsson H, Halldin C, Farde L. Quantification of ^{11}C-MADAM binding to the serotonin transporter in the human brain. *J Nucl Med.* 2005;46:1505–1515.
22. Farde L, Ito H, Swahn CG, Pike VW, Halldin C. Quantitative analyses of carbonyl-carbon-11-WAY-100635 binding to central 5-hydroxytryptamine-1A receptors in man. *J Nucl Med.* 1998;39:1965–1971.
23. Takano A, Suzuki K, Kosaka J, et al. A dose-finding study of duloxetine based on serotonin transporter occupancy. *Psychopharmacology (Berl).* 2006;185:395–399.
24. Arakawa R, Ito H, Takano A, et al. Dose-finding study of paliperidone ER based on striatal and extrastriatal dopamine D_2 receptor occupancy in patients with schizophrenia. *Psychopharmacology (Berl).* 2008;197:229–235.

Quantitative Analysis of NK_1 Receptor in the Human Brain Using PET with ^{18}F-FE-SPA-RQ

Masaki Okumura[1,2], Ryosuke Arakawa[1,2], Hiroshi Ito[1], Chie Seki[1], Hidehiko Takahashi[1], Harumasa Takano[1], Eisuke Haneda[1,3], Ryuji Nakao[4], Hidenori Suzuki[3], Kazutoshi Suzuki[4], Yoshiro Okubo[2], and Tetsuya Suhara[1]

[1]*Molecular Neuroimaging Group, Molecular Imaging Center, National Institute of Radiological Sciences, Chiba, Japan;* [2]*Department of Neuropsychiatry, Nippon Medical School, Tokyo, Japan;* [3]*Department of Pharmacology, Nippon Medical School, Tokyo, Japan; and* [4]*Molecular Probe Group, Molecular Imaging Center, National Institute of Radiological Sciences, Chiba, Japan*

^{18}F-fluoroethyl-SPA-RQ (^{18}F-FE-SPA-RQ) was recently developed as a radioligand for the measurement of neurokinin 1 (NK_1) receptor with PET. In this study, we used ^{18}F-FE-SPA-RQ with PET to visualize and quantify NK_1 receptor in the human brain. **Methods:** PET scans were performed on 7 healthy men after intravenous injection of ^{18}F-FE-SPA-RQ. Binding potential (BP_{ND}) was calculated by the indirect kinetic, simplified reference tissue model (SRTM), and ratio methods. The indirect kinetic method was used as the gold standard method and was compared with the SRTM method, with scan times of 180, 270, and 330 min, and with the ratio method, with time integration intervals of 120–180, 210–270, and 300–330 min. The cerebellum was used as the reference brain region. **Results:** Regional radioactivity was highest in the caudate head and putamen; mid level in the parahippocampus, cerebral cortex, and thalamus; and lowest in the cerebellum. BP_{ND} values by the indirect kinetic method were 3.15 ± 0.36, 3.11 ± 0.66, 1.17 ± 0.25, and 0.46 ± 0.14 in the caudate, putamen, parahippocampal region, and thalamus, respectively. For cerebral cortical regions, BP_{ND} values by the indirect kinetic method were 0.94 ± 0.23, 0.82 ± 0.15, 0.76 ± 0.15, and 0.69 ± 0.16 in the occipital, temporal, frontal, and anterior cingulate cortices, respectively. BP_{ND} values by the SRTM and ratio methods were in good agreement with those by the indirect kinetic method (r = 0.94–0.98). **Conclusion:** The regional distribution of ^{18}F-FE-SPA-RQ was in agreement with previous PET studies and postmortem studies of NK_1 receptor in the human brain. The ratio method will be useful for clinical research of psychiatric disorders, for the estimation of NK_1 receptor without arterial blood sampling and long dynamic PET.

Key Words: NK_1 receptor; substance P; ^{18}F-FE-SPA-RQ; PET; human brain

J Nucl Med 2008; 49:1749–1755
DOI: 10.2967/jnumed.108.054353

Tachykinins are a family of neuropeptides that serve as neurotransmitters in the central nervous system (CNS) and peripheral nervous system (PNS). Three major mammalian tachykinins—substance P (SP), neurokinin A, and neurokinin B—are known, and they share a consensus amino acid sequence (-Phe-X-Gly-Leu-Met-NH_2) in their carboxyl terminals (*1–4*). SP is a well-characterized neuropeptide, participating in neurotransmission by itself or synergistically with other neurotransmitters such as monoamines, acetylcholine, and glutamate in nerve terminals. Receptors for tachykinins—termed neurokinin 1 (NK_1), NK_2, and NK_3 receptors—have been identified (all are G protein–coupled 7-transmembrane receptors) and demonstrated to selectively show high affinity for SP, neurokinin A, and neurokinin B, respectively (*5,6*). NK_1 receptors are expressed in both CNS and PNS, whereas NK_2 and NK_3 receptors are expressed in PNS and CNS, respectively (*7,8*). SP and NK_1 receptors have been shown to play significant roles in pain (*9*), emesis (*10*), neuroinflammation (*11,12*), vasomotor control, and many gastrointestinal functions. Because the SP–NK_1 system is localized in brain regions (such as the striatum, amygdala, hypothalamus, raphe nucleus, and periaqueductal gray matter) that are involved in the regulation of affective behavior (*7,8*), the activity of the central tachykinergic pathway mediated by SP and NK_1 receptors is conceived to be mechanistically related to psychiatric conditions such as depression and anxiety disorder. Recent clinical trials of the NK_1 receptor antagonist aprepitant have shown that the blockade of SP is a highly effective strategy for the prevention of chemotherapy-induced nausea and vomiting (*13–15*). Aprepitant was recently registered worldwide, and it represents an improvement for antiemetic control during chemotherapy. Early clinical studies also suggested that aprepitant may have antidepressant activity, implicating SP in the modulation of mood and anxiety in humans (*16,17*). However, recent results from phase III clinical trials indicate that aprepitant is not effective for the treatment of depression (*18*).

A recently developed nonpeptide PET tracer that can permeate the blood–brain barrier, [^{18}F-2-fluoromethoxy-5-(5-trifluoromethyl-tetrazol-1-yl)-benzyl]([2S,3S]2-phenyl-piperidin-3-yl)-amine) (^{18}F-SPA-RQ) (*19*), has been proven

Received May 14, 2008; revision accepted Jul. 14, 2008.
For correspondence or reprints contact: Hiroshi Ito, Molecular Neuroimaging Group, Molecular Imaging Center, National Institute of Radiological Sciences 4-9-1, Anagawa, Inage-ku, Chiba, 263-8555, Japan.
E-mail: hito@nirs.go.jp

to bind to NK_1 receptors with high affinity and selectivity and applied to in vivo imaging of human brains (*20–22*).

^{18}F-fluoroethyl-SPA-RQ (^{18}F-FE-SPA-RQ) was recently developed as a radioligand for the measurement of NK_1 receptors (*23*). It is the fluoroethyl analog of ^{18}F-SPA-RQ and was designed for brain imaging with reduced radioactive accumulation in bone by slowing the rate of defluorination. ^{18}F-FE-SPA-RQ has higher affinity for NK_1 receptors than does ^{18}F-SPA-RQ (human NK_1 inhibitory concentration of 50% [IC_{50}] = 17 and 67 pM for ^{18}F-FE-SPA-RQ and ^{18}F-SPA-RQ, respectively), and a small-animal PET study has been performed using ^{18}F-FE-SPA-RQ (*24*). In the present study, we aimed to quantify NK_1 receptor binding in the human brain using ^{18}F-FE-SPA-RQ with arterial blood sampling and also to validate noninvasive methods for the quantification without arterial blood sampling.

MATERIALS AND METHODS

Subjects

A total of 7 healthy male subjects (age range, 20–31 y; mean ± SD, 24.6 ± 4.0 y) participated in this study. All subjects were free of any somatic, neurologic, or psychiatric disorders, and they had no history of current or previous drug abuse. After we described the study to the participants, written informed consent was obtained. The study was approved by the Ethics and Radiation Safety Committee of the National Institute of Radiologic Sciences, Chiba, Japan.

Radioligand

The NK_1 receptor antagonist SPA-RQ (molecular weight, 450M) was labeled with the positron emitter ^{18}F (half-life, 109.8 min). Details of the precursor compound, radiosynthesis, and quality control were described previously (*23,25*). Briefly, ^{18}F-FCH_2CH_2Br was prepared from ^{18}F-F^- and 2-bromoethyl triflate and purified by distillation. ^{18}F-Fluoroalkylation of the deprotonated phenolic hydroxyl group in the precursor with FCH_2CH_2Br in dimethyl formamide was performed at 120°C for 10 min. The resultant ^{18}F-FE-SPA-RQ was purified by preparative high-performance liquid chromatography (HPLC). The final product was formulated in saline solution (10 mL) containing polysorbate 80 (75 μL).

PET Procedure

A PET scanner system (ECAT EXACT HR+; CTI-Siemens) was used for all subjects, and a head restraint was used to minimize head movement. A transmission scan for attenuation correction was performed using a ^{68}Ge–^{68}Ga source, and a dynamic PET scan was performed after a 1-min intravenous slow-bolus injection of 210.2–228.8 MBq (221.6 ± 6.7 MBq) of ^{18}F-FE-SPA-RQ. Specific radioactivity of ^{18}F-FE-SPA-RQ was 281.8–487.7 GBq/μmol (355.6 ± 68.7 GBq/μmol). Brain radioactivity was measured from 0 to 90 min (1 min × 10, 2 min × 15, 5 min × 10), from 120 to 180 min (5 min × 12), from 210 to 270 min (5 min × 12), and from 300 to 330 min (5 min × 6). MR images of the brain were acquired with a 1.5-T MRI scanner (Gyroscan NT; Philips). T1-weighted images were obtained at 1-mm slices.

Arterial Blood Sampling and Metabolite Analysis

To obtain the arterial input function, arterial blood samples were taken manually 49 times during PET. Each of the blood samples was centrifuged to obtain plasma and blood cell fractions, and the concentrations of radioactivity in whole blood and in plasma were measured.

The percentage of unchanged ^{18}F-FE-SPA-RQ in plasma was determined by HPLC in 29 of the total blood samples. Acetonitrile was added to each plasma sample, and samples were centrifuged. The supernatant was subjected to radio-HPLC analysis using an XBridge Prep C18 column (Waters) (mobile phase, 6:4 90% acetonitrile:50 mM phosphoric acid). The plasma input function was defined as the radioactivity of plasma multiplied by the percentage of unchanged radioligand. Plasma protein binding was not determined in the present study.

Regions of Interest

All MR images were coregistered to the PET images using a statistical parametric mapping (SPM2) system. Regions of interest were drawn manually on summated PET images with reference to coregistered MRI and were defined for the caudate head; putamen; parahippocampal region; occipital, temporal, frontal, and anterior cingulate cortices; thalamus; and cerebellum, according to our previous study (*26*). The parahippocampal region included the hippocampus, posterior part of the parahippocampal gyrus, and uncus including the amygdala. Regional radioactivity was calculated for each frame, corrected for decay, and plotted versus time.

Kinetics Model of ^{18}F-FE-SPA-RQ

The 3-compartment model (3CM) with 4 first-order rate constants was used to describe the kinetics of ^{18}F-FE-SPA-RQ in the brain. The 3 compartments were defined as follows: C_P, the radioactivity concentration of unchanged radioligand in plasma (arterial input function); C_{ND}, the radioactivity concentration of nondisplaceable radioligand in the brain, including nonspecifically bound and free radioligand; and C_S, the radioactivity concentration of radioligand specifically bound to receptors. The rate constants K_1 and k_2 represent the influx and efflux rates for radioligand diffusion through the blood–brain barrier, respectively. The rate constants k_3 and k_4 are the radioligand transfers between the compartments for nondisplaceable and specifically bound radioligand. This model can be described by the following equations:

$$dC_{ND}(t)/dt = K_1C_P(t) - (k_2 + k_3)C_{ND}(t) + k_4C_S(t),$$

$$dC_S(t)/dt = k_3C_{ND}(t) - k_4C_S(t), \text{ and}$$

$$C_T(t) = C_{ND}(t)+C_S(t).$$

$C_T(t)$ is the total radioactivity concentration in a brain region measured by PET.

Calculation of ^{18}F-FE-SPA-RQ Binding Potential (BP_{ND})

^{18}F-FE-SPA-RQ binding was quantified by the indirect kinetic, simplified reference tissue model (SRTM), and ratio methods. In these methods, ^{18}F-FE-SPA-RQ bindings were expressed as BP_{ND} relative to nondisplaceable bindings (*27*). We used the cerebellum as reference brain region because of its negligible NK_1 receptor

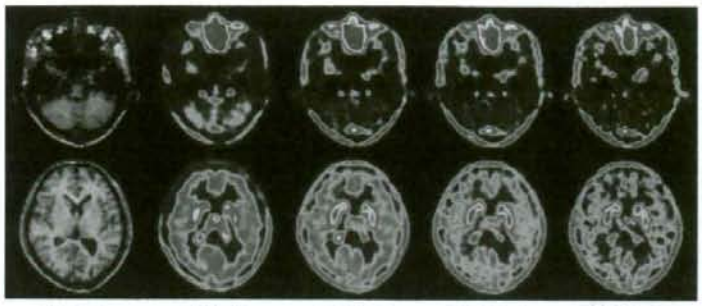

FIGURE 1. Typical summated PET images of ^{18}F-FE-SPA-RQ and T1-weighted MR images. Upper row shows slice of cerebellum, and lower row shows slice of caudate, putamen, and cerebral cortex.

density (*20,22,28*). For these analyses, the software package PMOD (PMOD Technologies) was used.

Indirect Kinetic Method. With the cerebellum as reference region, BP_{ND} can be expressed as:

$$BP_{ND} = V_{T(regions)}/V_{T(cerebellum)} - 1,$$

where $V_{T(regions)}$ is the total distribution volume ($= [K_1/k_2][k_3/k_4 + 1]$) of target regions and $V_{T(cerebellum)}$ is that of the cerebellum. K_1, k_2, k_3, and k_4 values were determined by nonlinear least-squares curve fitting to the regional time–activity curves. In this analysis, blood volume (V_b), which depends on the first-pass extraction fraction of the tracer, was assumed to be 0.04 mL/mL, with use of the radioactivity of whole blood to diminish the influence of the tracer remaining in the blood. In this study, the indirect kinetic method was used as the gold standard method (*29*).

SRTM Method. Assuming that both target and reference regions have the same level of nondisplaceable binding, the SRTM can be used to describe time–activity data in the target region as follows (*30*):

$$C_T(t) = R_1C_R(t) + (k_2 - R_1k_2/[1+BP_{ND}])C_R(t)* \exp(-k_2t/[1+BP_{ND}]),$$

where R_1 is the ratio of K_1/K_1' (K_1, influx rate constant for the brain region; K_1', influx rate constant for the reference region), $C_R(t)$ is the radioactivity concentration in the reference region (cerebellum), and * denotes the convolution integral. Using this method, 3 parameters (R_1, k_2, and BP_{ND}) were estimated by a nonlinear curve-fitting procedure. Scan data up to 180, 270, and 330 min were used.

Ratio Method. In the ratio method, BP_{ND} can be expressed as:

$$BP_{ND} = AUC_{(regions)}/AUC_{(cerebellum)} - 1,$$

where $AUC_{(regions)}$ is the area under the time–activity curve of target regions and $AUC_{(cerebellum)}$ is the time–activity curve of the cerebellum. The integration intervals of 120–180, 210–270, and 300–330 min were used.

RESULTS

Typical summated PET images of 4 time periods and T1-weighted MR images are shown in Figure 1. Typical time–activity curves in the brain showed that regional radioactivity was highest in the putamen and caudate (Fig. 2). The next highest region was the parahippocampus, followed by the cerebral cortices and thalamus. Among cerebral

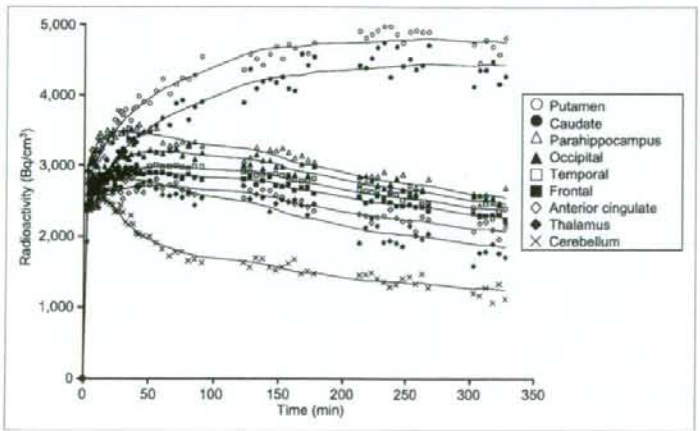

FIGURE 2. Typical time–activity curves of ^{18}F-FE-SPA-RQ in brain. Time–activity curves of all regions could be described by 3CM.

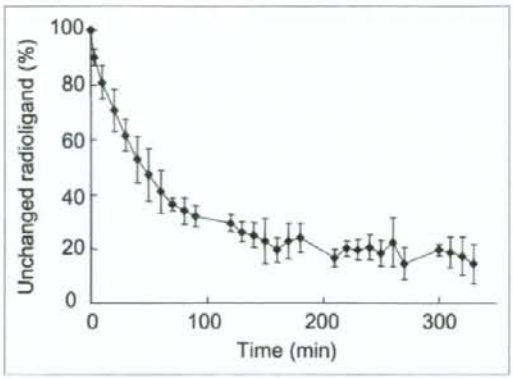

FIGURE 3. Average percentage of unchanged ^{18}F-FE-SPA-RQ in plasma. Bars indicate 1 SD.

cortices, the occipital cortex showed the highest radioactivity. Lowest radioactivity was shown in the cerebellum.

In this study, the fraction of unchanged ^{18}F-FE-SPA-RQ in plasma could not be measured by HPLC analysis in 3 of the 7 subjects because of low radioactivity in blood samples. So, the average of the fractions of unchanged ^{18}F-FE-SPA-RQ in plasma of the other 4 subjects was used for these 3 subjects for the indirect kinetic method. The average percentage fraction of unchanged ^{18}F-FE-SPA-RQ in plasma of the 4 subjects was 90.0% ± 2.9% at 3 min, 80.9% ± 6.1% at 10 min, 32.0% ± 3.9% at 90 min, 23.9% ± 5.3% at 180 min, 14.6% ± 5.9% at 270 min, and 14.4% ± 7.3% at 330 min (Fig. 3).

The rate constants for the 9 regions determined by the kinetic approach using the 3CM with arterial input function are shown in Table 1. For the cerebellum, the 2-compartment model (2CM) without specific binding compartment was also used. Akaike information criteria of the 3CM were significantly lower than those of the 2CM in the cerebellum (290 ± 28 vs. 409 ± 25, $P < 0.0001$; paired t statistics).

The BP_{ND} values of all brain regions calculated by all methods are shown in Table 2. BP_{ND} values by the SRTM method with a scan time of 330 min showed the best correlation with those by the indirect kinetic method (r = 0.98) (Fig. 4A). The SRTM method with scan times of 270 and 180 min and the ratio method with time integration intervals of 300–330, 210–270, and 120–180 min were also in good agreement with the indirect kinetic method in BP_{ND} values (r = 0.94–0.97) (Figs. 4B and 4C; Fig. 5). The BP_{ND} values, except for the caudate and putamen by the SRTM method with a scan time of 180 min and the ratio method with a time integration interval of 120–180 min, were also in good agreement with the indirect kinetic method (SRTM, $r = 0.94$, $y = 0.70x + 0.20$; ratio method, $r = 0.94$, $y = 0.69x + 0.20$).

The BP_{ND} values determined by the kinetic approach ($= k_3/k_4$) were 4.39 ± 3.93 and 5.94 ± 3.44 in the caudate and putamen. Those in the other regions were much smaller and varied widely.

DISCUSSION

After the intravenous injection of ^{18}F-FE-SPA-RQ, radioactivity was highest in the caudate and putamen and lowest in the cerebellum. BP_{ND} values in the caudate and putamen by the indirect kinetic method were 3.15 ± 0.36 and 3.11 ± 0.66, respectively, almost the same as in the previous human PET study with ^{18}F-SPA-RQ (3.08 ± 0.48 in the caudate and 3.71 ± 1.00 in the putamen) (*22*). The parahippocampal region and cerebral cortices showed moderate uptake, and the occipital cortex showed the highest uptake among the cerebral cortices. The thalamus showed relatively low uptake. The uptake shown in these regions was almost the same order of progression as the uptake in previous human PET studies with ^{18}F-SPA-RQ and autoradiographic studies of the human postmortem brain

TABLE 1
Rate Constants for Each Brain Region Determined by Kinetic Approach Using 3CM with Arterial Input Function

Region	Rate constant				Total distribution volume
	K_1 (mL/mL/min)	k_2 (min^{-1})	k_3 (min^{-1})	k_4 (min^{-1})	
Putamen	0.111 ± 0.019	0.036 ± 0.016	0.081 ± 0.040	0.014 ± 0.003	21.3 ± 3.4
Caudate	0.088 ± 0.018	0.023 ± 0.018	0.061 ± 0.067	0.011 ± 0.005	21.5 ± 1.7
Parahippocampus	0.140 ± 0.023	0.033 ± 0.007	0.027 ± 0.020	0.015 ± 0.006	11.3 ± 1.4
Occipital lobe	0.127 ± 0.017	0.065 ± 0.038	0.089 ± 0.057	0.021 ± 0.007	10.0 ± 1.1
Temporal lobe	0.106 ± 0.050	0.050 ± 0.025	0.067 ± 0.038	0.020 ± 0.003	9.5 ± 0.9
Frontal lobe	0.108 ± 0.011	0.041 ± 0.011	0.052 ± 0.023	0.021 ± 0.002	9.1 ± 0.9
Anterior cingulate cortex	0.115 ± 0.014	0.064 ± 0.018	0.072 ± 0.027	0.019 ± 0.005	8.8 ± 0.9
Thalamus	0.112 ± 0.019	0.043 ± 0.018	0.038 ± 0.026	0.019 ± 0.003	7.6 ± 0.9
Cerebellum					
3CM	0.115 ± 0.017	0.051 ± 0.015	0.017 ± 0.008	0.013 ± 0.003	5.2 ± 0.4
2CM	0.089 ± 0.014	0.019 ± 0.002			4.6 ± 0.3

Values are mean ± SD. For cerebellum, both 2CM and 3CM were applied.

TABLE 2
BP_{ND} Values for Each Brain Region with All Methods

Region	Method						
		SRTM (min)			Ratio (min)		
	Indirect kinetic	330	270	180	300–330	210–270	120–180
Putamen	3.11 ± 0.66	2.43 ± 0.33	2.33 ± 0.32	2.20 ± 0.27	2.62 ± 0.40	2.25 ± 0.28	1.81 ± 0.19
Caudate	3.15 ± 0.36	2.14 ± 0.24	2.02 ± 0.22	1.91 ± 0.20	2.31 ± 0.40	1.98 ± 0.26	1.57 ± 0.17
Parahippocampus	1.17 ± 0.25	1.04 ± 0.16	1.02 ± 0.12	1.01 ± 0.12	1.11 ± 0.22	1.05 ± 0.16	1.03 ± 0.20
Occipital lobe	0.94 ± 0.23	0.88 ± 0.14	0.92 ± 0.07	0.90 ± 0.13	0.97 ± 0.16	0.94 ± 0.16	0.95 ± 0.17
Temporal lobe	0.82 ± 0.15	0.77 ± 0.11	0.79 ± 0.08	0.78 ± 0.11	0.85 ± 0.15	0.83 ± 0.15	0.79 ± 0.15
Frontal lobe	0.76 ± 0.15	0.72 ± 0.12	0.74 ± 0.07	0.73 ± 0.11	0.79 ± 0.17	0.76 ± 0.15	0.75 ± 0.15
Anterior cingulate cortex	0.69 ± 0.16	0.66 ± 0.15	0.67 ± 0.13	0.71 ± 0.17	0.70 ± 0.16	0.69 ± 0.13	0.67 ± 0.13
Thalamus	0.46 ± 0.14	0.46 ± 0.13	0.51 ± 0.10	0.49 ± 0.14	0.45 ± 0.12	0.45 ± 0.13	0.49 ± 0.16

Values are mean ± SD.

(*20,22,28*). In a previous autoradiographic study using ^{3}H-GR205171, the maximum number of binding sites for NK_1 receptor in the striatum was 6 times as much as in the cortex (*31*), a result in accordance with the BP_{ND} values in these regions in the present study.

In this study, the indirect kinetic method with arterial blood sampling was used as the gold standard method, because BP_{ND} determined by the kinetic approach as k_3/k_4 showed wide variation. The BP_{ND} values in all brain regions determined by the SRTM method (with scan times of 330, 270, and 180 min) and by the ratio method (with time integration intervals of 300–330, 210–270, and 120–180 min) were in good agreement with those determined by the indirect kinetic method. Although good correlations were observed in BP_{ND} values among the methods, BP_{ND} was underestimated in the caudate and putamen using the

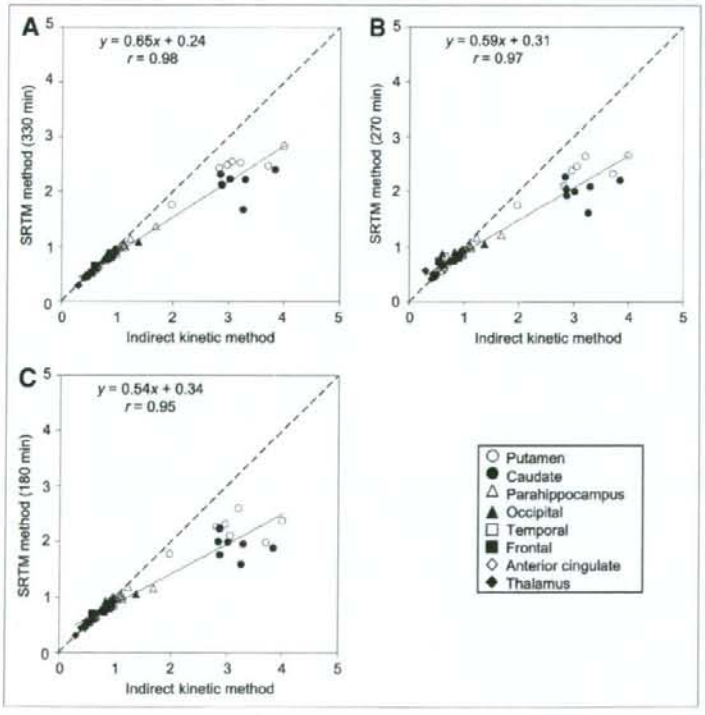

FIGURE 4. Correlation among BP_{ND} values in all brain regions estimated by indirect kinetic and SRTM methods, with scan times of 330 (A), 270 (B), and 180 (C) min.

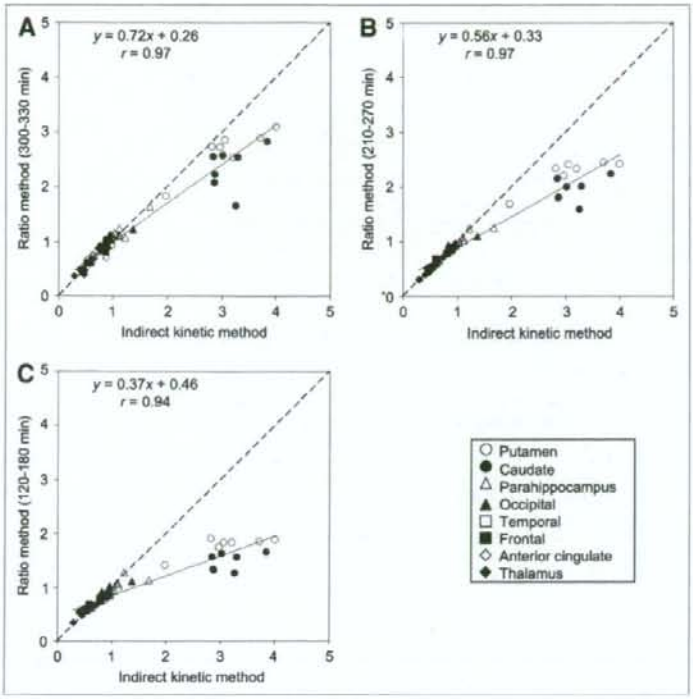

FIGURE 5. Correlation among BP_{ND} values in all brain regions estimated by indirect kinetic and ratio methods, with time integration intervals of 300–330 (A), 210–270 (B), and 120–180 (C) min.

SRTM and ratio methods. The underestimations of BP_{ND} were 32% and 34% in the caudate and 22% and 16% in the putamen for the SRTM method (with a scan time of 330 min) and the ratio method (with a time integration interval of 300–330 min), respectively. More underestimation was observed in the caudate and putamen with the shorter scan time in the SRTM method and with the earlier time integration interval in the ratio method. The reason might be that striatal radioactivity in some subjects did not reach a peak by 330 min. However, the BP_{ND} values of the other regions calculated by the SRTM method (with a scan time of 180 min) and the ratio method (with a time integration interval of 120–180 min) were not greatly underestimated, indicating that the scan time can be shortened to 180 min. Although the indirect kinetic method was considered as the gold standard method, it required a long PET time and arterial blood sampling, an invasive procedure sometimes difficult for patients with psychiatric disorders. The ratio method, which does not require a long PET scanning time and arterial blood sampling, would surely be preferable for clinical investigations. The ratio method, with a time integration interval of 300–330 min, seemed most suitable because the correlation coefficient with the indirect kinetic method was highest and the slope of the regression line was nearest to 1.

The time–activity curves in the cerebellum were well described by the 3CM rather than the 2CM. Similar results were reported for several PET radioligands, with the kinetics in the reference region also being evaluated using the 3CM (*29,32,33*). The results could be explained if the cerebellum would contain specific bindings for NK_1 receptors. However, previous autoradiographic studies showed that the density of NK_1 receptors in the cerebellum was low (*22*), and a previous PET study with ^{18}F-SPA-RQ showed that there was no change in the cerebellar signal before and after high blocking doses of the NK_1 receptor antagonist aprepitant (*20*). Another possible explanation for the results was that the compartments of free and nonspecific binding might have been separated by the kinetic analysis. In addition, ^{18}F-FE-SPA-RQ showed defluorination during the later scans, and bone uptake of ^{18}F might influence the radioactivity in the cerebral cortex and cerebellum adjacent to the skull (although ^{18}F-FE-SPA-RQ showed reduced radioactive accumulation in bone, compared with ^{18}F-SPA-RQ (*23*)).

CONCLUSION

^{18}F-FE-SPA-RQ is a suitable radioligand for PET measurement of NK_1 receptors in the human brain. The 3CM could well describe the brain kinetics of ^{18}F-FE-SPA-RQ. Because the ratio method does not require long scanning times and arterial blood sampling, this method would be useful for clinical research on psychiatric disorders.

ACKNOWLEDGMENTS

We thank Dr. Fumitoshi Kodaka, Dr. Tatsui Otsuka, Katsuyuki Tanimoto, Takahiro Shiraishi, and Akira Ando for their assistance in performing the PET experiments at the National Institute of Radiological Sciences. We also thank Yoshiko Fukushima of the National Institute of Radiological Sciences for her help as clinical research coordinator. This study was supported by a consignment expense for the Molecular Imaging Program on Research Base for PET Diagnosis from the Ministry of Education, Culture, Sports, Science and Technology (MEXT), Japanese Government.

REFERENCES

1. Baker KG, Halliday GM, Hornung JP, Geffen LB, Cotton RG, Tork I. Distribution, morphology and number of monoamine-synthesizing and substance P-containing neurons in the human dorsal raphe nucleus. *Neuroscience*. 1991; 42:757–775.
2. Nicholas AP, Pieribone VA, Arvidsson U, Hokfelt T. Serotonin-, substance P- and glutamate/aspartate-like immunoreactivities in medullo-spinal pathways of rat and primate. *Neuroscience*. 1992;48:545–559.
3. Sergeyev V, Hokfelt T, Hurd Y. Serotonin and substance P co-exist in dorsal raphe neurons of the human brain. *Neuroreport*. 1999;10:3967–3970.
4. Vincent SR, Satoh K, Armstrong DM, Panula P, Vale W, Fibiger HC. Neuropeptides and NADPH-diaphorase activity in the ascending cholinergic reticular system of the rat. *Neuroscience*. 1986;17:167–182.
5. Masu Y, Nakayama K, Tamaki H, Harada Y, Kuno M, Nakanishi S. cDNA cloning of bovine substance-K receptor through oocyte expression system. *Nature*. 1987;329:836–838.
6. Nakanishi S. Mammalian tachykinin receptors. *Annu Rev Neurosci*. 1991; 14:123–136.
7. Ding YQ, Shigemoto R, Takada M, Ohishi H, Nakanishi S, Mizuno N. Localization of the neuromedin K receptor (NK_3) in the central nervous system of the rat. *J Comp Neurol*. 1996;364:290–310.
8. Nakaya Y, Kaneko T, Shigemoto R, Nakanishi S, Mizuno N. Immunohistochemical localization of substance P receptor in the central nervous system of the adult rat. *J Comp Neurol*. 1994;347:249–274.
9. Snider WD, McMahon SB. Tackling pain at the source: new ideas about nociceptors. *Neuron*. 1998;20:629–632.
10. Sanger GJ. Neurokinin NK_1 and NK_3 receptors as targets for drugs to treat gastrointestinal motility disorders and pain. *Br J Pharmacol*. 2004;141:1303–1312.
11. Kincy-Cain T, Bost KL. Increased susceptibility of mice to Salmonella infection following in vivo treatment with the substance P antagonist, spantide II. *J Immunol*. 1996;157:255–264.
12. Metwali A, Blum AM, Elliott DE, Setiawan T, Weinstock JV. Cutting edge: hemokinin has substance P-like function and expression in inflammation. *J Immunol*. 2004;172:6528–6532.
13. Hesketh PJ, Van Belle S, Aapro M, et al. Differential involvement of neurotransmitters through the time course of cisplatin-induced emesis as revealed by therapy with specific receptor antagonists. *Eur J Cancer*. 2003; 39:1074–1080.
14. Hesketh PJ, Grunberg SM, Gralla RJ, et al. The oral neurokinin-1 antagonist aprepitant for the prevention of chemotherapy-induced nausea and vomiting: a multinational, randomized, double-blind, placebo-controlled trial in patients receiving high-dose cisplatin—the Aprepitant Protocol 052 Study Group. *J Clin Oncol*. 2003;21:4112–4119.
15. de Wit R, Herrstedt J, Rapoport B, et al. Addition of the oral NK1 antagonist aprepitant to standard antiemetics provides protection against nausea and vomiting during multiple cycles of cisplatin-based chemotherapy. *J Clin Oncol*. 2003;21:4105–4111.
16. Kramer MS, Cutler N, Feighner J, et al. Distinct mechanism for antidepressant activity by blockade of central substance P receptors. *Science*. 1998;281:1640–1645.
17. Kramer MS, Winokur A, Kelsey J, et al. Demonstration of the efficacy and safety of a novel substance P (NK_1) receptor antagonist in major depression. *Neuropsychopharmacology*. 2004;29:385–392.
18. Keller M, Montgomery S, Ball W, et al. Lack of efficacy of the substance p (neurokinin1 receptor) antagonist aprepitant in the treatment of major depressive disorder. *Biol Psychiatry*. 2006;59:216–223.
19. Solin O, Eskola O, Hamill TG, et al. Synthesis and characterization of a potent, selective, radiolabeled substance-P antagonist for NK_1 receptor quantitation: ([^{18}F]SPA-RQ). *Mol Imaging Biol*. 2004;6:373–384.
20. Bergstrom M, Hargreaves RJ, Burns HD, et al. Human positron emission tomography studies of brain neurokinin 1 receptor occupancy by aprepitant. *Biol Psychiatry*. 2004;55:1007–1012.
21. Hargreaves R. Imaging substance P receptors (NK_1) in the living human brain using positron emission tomography. *J Clin Psychiatry*. 2002;63(suppl 11):S18–S24.
22. Hietala J, Nyman MJ, Eskola O, et al. Visualization and quantification of neurokinin-1 (NK_1) receptors in the human brain. *Mol Imaging Biol*. 2005; 7:262–272.
23. Hamill T, Ryan C, Krause S, et al. The synthesis and in vivo characterization of [^{18}F]FESPARQ, a neurokinin-1 (NK_1) receptor PET ligand [abstract]. *J Labelled Comp Radiopharm*. 2003;46(suppl 1):S35.
24. Haneda E, Higuchi M, Maeda J, et al. In vivo mapping of substance P receptors in brains of laboratory animals by high-resolution imaging systems. *Synapse*. 2007;61:205–215.
25. Zhang MR, Maeda J, Furutsuka K, et al. [^{18}F]FMDAA1106 and [^{18}F]FE-DAA1106: two positron-emitter labeled ligands for peripheral benzodiazepine receptor (PBR). *Bioorg Med Chem Lett*. 2003;13:201–204.
26. Ito H, Takahashi H, Arakawa R, Takano H, Suhara T. Normal database of dopaminergic neurotransmission system in human brain measured by positron emission tomography. *Neuroimage*. 2008;39:555–565.
27. Innis RB, Cunningham VJ, Delforge J, et al. Consensus nomenclature for in vivo imaging of reversibly binding radioligands. *J Cereb Blood Flow Metab*. 2007;27:1533–1539.
28. Caberlotto L, Hurd YL, Murdock P, et al. Neurokinin 1 receptor and relative abundance of the short and long isoforms in the human brain. *Eur J Neurosci*. 2003;17:1736–1746.
29. Ito H, Sudo Y, Suhara T, Okubo Y, Halldin C, Farde L. Error analysis for quantification of [^{11}C]FLB 457 binding to extrastriatal D_2 dopamine receptors in the human brain. *Neuroimage*. 2001;13:531–539.
30. Lammertsma AA, Hume SP. Simplified reference tissue model for PET receptor studies. *Neuroimage*. 1996;4:153–158.
31. Griffante C, Carletti R, Andreetta F, Corsi M. [^{3}H]GR205171 displays similar NK_1 receptor binding profile in gerbil and human brain. *Br J Pharmacol*. 2006; 148:39–45.
32. Farde L, Ito H, Swahn CG, Pike VW, Halldin C. Quantitative analyses of carbonyl-carbon-11-WAY-100635 binding to central 5-hydroxytryptamine-1A receptors in man. *J Nucl Med*. 1998;39:1965–1971.
33. Lundberg J, Odano I, Olsson H, Halldin C, Farde L. Quantification of ^{11}C-MADAM binding to the serotonin transporter in the human brain. *J Nucl Med*. 2005;46:1505–1515.

Behavioral/Systems/Cognitive

Differential Contributions of Prefrontal and Hippocampal Dopamine D_1 and D_2 Receptors in Human Cognitive Functions

Hidehiko Takahashi,[1] Motoichiro Kato,[2] Harumasa Takano,[1] Ryosuke Arakawa,[1] Masaki Okumura,[1] Tatsui Otsuka,[1] Fumitoshi Kodaka,[1] Mika Hayashi,[2] Yoshiro Okubo,[3] Hiroshi Ito,[1] and Tetsuya Suhara[1]

[1]Molecular Imaging Center, Department of Molecular Neuroimaging, National Institute of Radiological Sciences, Inage, Chiba 263-8555, Japan, [2]Department of Neuropsychiatry, Keio University School of Medicine, Shinjuku-ku, Tokyo 160-8582, Japan, and [3]Department of Neuropsychiatry, Nippon Medical School, Bunkyo-ku, Tokyo 113-8603, Japan

Dopamine D_1 receptors in the prefrontal cortex (PFC) are important for prefrontal functions, and it is suggested that stimulation of prefrontal D_1 receptors induces an inverted U-shaped response, such that too little or too much D_1 receptor stimulation impairs prefrontal functions. Less is known of the role of D_2 receptors in cognition, but previous studies showed that D_2 receptors in the hippocampus (HPC) might play some roles via HPC–PFC interactions. We measured both D_1 and D_2 receptors in PFC and HPC using positron emission tomography in healthy subjects, with the aim of elucidating how regional D_1 and D_2 receptors are differentially involved in frontal lobe functions and memory. We found an inverted U-shaped relation between prefrontal D_1 receptor binding and Wisconsin Card Sorting Test performance. However, prefrontal D_2 binding has no relation with any neuropsychological measures. Hippocampal D_2 receptor binding showed positive linear correlations not only with memory function but also with frontal lobe functions, but hippocampal D_1 receptor binding had no association with any memory and prefrontal functions. Hippocampal D_2 receptors seem to contribute to local hippocampal functions (long-term memory) and to modulation of brain functions outside HPC ("frontal lobe functions"), which are mainly subserved by PFC, via the HPC–PFC pathway. Our findings suggest that orchestration of prefrontal D_1 receptors and hippocampal D_2 receptors might be necessary for human executive function including working memory.

Key words: dopamine; D_1 receptors; D_2 receptors; prefrontal cortex; hippocampus; positron emission tomography

Introduction

Because dopamine D_1 receptors in the prefrontal cortex (PFC) are several times more abundant than D_2 receptors (Hall et al., 1994), the relationship between D_1 receptors and PFC functions have been widely investigated. Sawaguchi and Goldman-Rakic (1994) demonstrated that local administration of D_1 receptor antagonists into PFC induced impairment in working memory task in nonhuman primate. In human, Müller et al. (1998) reported that systemic administration of a mixed D_1/D_2 agonist facilitated working memory, whereas the selective D_2 agonist had no effect, indicating that the dopaminergic modulation of working memory processes is mediated primarily via D_1 receptors. The use of positron emission tomography (PET) allows us to quantify dopamine receptors *in vivo*, and previous studies reported that altered prefrontal D_1 receptors in schizophrenia were associated with working memory deficits (Okubo et al., 1997; Abi-Dargham et al., 2002).

In contrast to D_1 receptors, relatively less attention has been paid to the role of prefrontal D_2 receptors in cognitive functions. It was reported that blockade of D_2 receptors in PFC did not impair working memory in nonhuman primate (Sawaguchi and Goldman-Rakic, 1994), but some human studies reported that systemic administration of D_2 agonist or antagonist modulated cognitive functions that are subserved by the prefrontal cortex (McDowell et al., 1998; Mehta et al., 1999). Because the density of D_2 receptors in extrastriatal regions is very low (Suhara et al., 1999), PET studies investigating the involvement of extrastriatal D_2 receptors in cognition have been limited. With the introduction of high-affinity PET radioligands such as [^{11}C]FLB457, it has become possible to quantify extrastriatal D_2 receptors by PET (Halldin et al., 1995). Using [^{11}C]FLB457, Kemppainen et al. (2003) reported that a reduction of D_2 receptors in the hippocampus (HPC) in Alzheimer's disease patients was correlated with memory impairments. Our recent PET study also showed that D_2 receptors in HPC were associated not only with memory function but also with frontal lobe functions (Takahashi et al., 2007), suggesting dopaminergic modulation on HPC–PFC inter-

Received July 23, 2008; revised Sept. 2, 2008; accepted Oct. 2, 2008.

This work was supported by a consignment expense for Molecular Imaging Program on "Research Base for PET Diagnosis" from the Ministry of Education, Culture, Sports, Science, and Technology (MEXT), the Japanese Government, and a Grant-in-Aid for Scientific Research from MEXT (18/90858). We thank Katsuyuki Tanimoto, Takahiro Shirashi, and Toshio Miyamoto for their assistance in performing the PET experiments at the National Institute of Radiological Sciences. We also thank Yoshiko Fukushima of the National Institute of Radiological Sciences for her help as clinical research coordinator.

Correspondence should be addressed to Dr. Hidehiko Takahashi, Department of Molecular Neuroimaging, National Institute of Radiological Sciences, 9-1, 4-chome, Anagawa, Inage-ku, Chiba, Chiba 263-8555, Japan. E-mail: hidehiko@nirs.go.jp.

DOI: 10.1523/JNEUROSCI.3446-08.2008

 0270-6474/08/2812032-07$15.00/0